Science of the Total Environment 953 (2024) 176016

Contents lists available at ScienceDirect

Science of the Total Environment

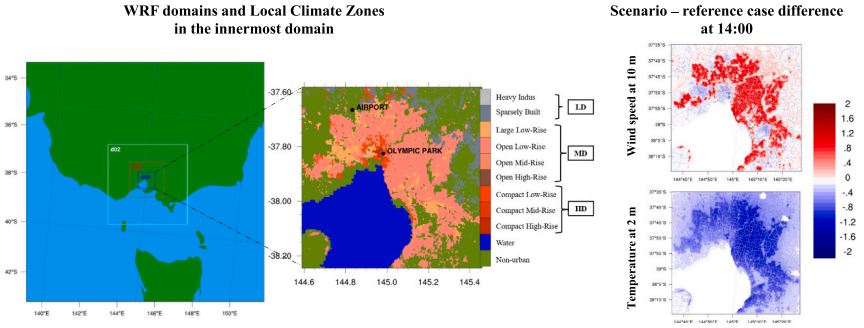
journal homepage: www.elsevier.com/locate/scitotenv

Investigating the effects of the greenery increase on air temperature, ventilation and cooling energy demand in Melbourne with the Weather Research and Forecasting model and Local Climate Zones

Serena Falasca [a,*], Michele Zinzi [b], Anna Maria Siani [a], Gabriele Curci [c,d], Lan Ding [e], Mattheos Santamouris [e]

[a] Department of Physics, "Sapienza" University of Rome, Piazzale Aldo Moro 5, 00185 Rome, Italy
[b] ENEA-Italian National Agency for New Technologies, Energy and Sustainable Economic Development, Italy
[c] Department of Physical and Chemical Sciences (DSFC), University of L'Aquila, 67100 L'Aquila, Italy
[d] Center of Excellence for the Remote Sensing and Forecast of Severe Weather (CETEMPS), Department of Physical and Chemical Sciences, University of L'Aquila, L'Aquila, Italy
[e] School of Built Environment, University of New South Wales, Sydney, Australia

GRAPHICAL ABSTRACT



ARTICLE INFO

Editor: Jurgen Mahlknecht

Keywords:
Urban Heat Island
Mitigation

ABSTRACT

Vegetation has a well-known potential for mitigating urban overheating. This work aims to explore the effects of enhancing urban greenery in Melbourne (Australia) through a configuration of the Weather Research and Forecasting (WRF) model including the Building Effect Parameterization and the Local Climate Zones and presents novelties in: i) covering two-months and ii) focusing on air circulation and buildings cooling energy demand through the ventilation coefficient (VC) and the cooling degree hours (CDHs). A control case and two

Abbreviations: BEP, Building Effect Parameterization; CDHs, Cooling Degree Hours; CTRL, control case; FAC2, fraction of predictions within a factor of two of observations; FB, Fractional Bias; gr50, modest increase scenario, with average urban green equal to 50 %; gr65, robust increase scenario, with average urban green equal to 65 %; HD, High Density; HW, Heat Wave; LCZ, Local Climate Zone; LD, Low Density; LT, Local Time; MB, Mean Bias; MD, Middle Density; NMSE, Normalized Mean Square Error; PBL, Planetary Boundary Layer; PBLH, Planetary Boundary Layer Height; R, Pearson correlation coefficient; SLUCM, Single Layer Urban Canopy Model; T2, air temperature at 2 m height; UHI, Urban Heat Island; VC, Ventilation Coefficient; WRF, Weather Research and Forecasting model; WS, wind speed; WS10, wind speed at 10 m height; WUDAPT, World Urban Database and Access Portal Tools.

* Corresponding author at: Department of Physics, Sapienza University of Rome, Piazzale Aldo Moro 5, 00185 Rome, Italy.
E-mail address: serena.falasca@uniroma1.it (S. Falasca).

https://doi.org/10.1016/j.scitotenv.2024.176016
Received 29 December 2023; Received in revised form 22 July 2024; Accepted 2 September 2024
Available online 4 September 2024
0048-9697/© 2024 The Authors. Published by Elsevier B.V. This is an open access article under the CC BY license (http://creativecommons.org/licenses/by/4.0/).

Urban climate
Urban vegetation
WRF
WUDAPT

"what-if" scenarios with a growing green coverage equal to 35 % (control case), 50 % (modest increase) and 60 % (robust increase) have been designed and then simulated for January and February 2019. Outcomes reveal a maximum drop in 2 m temperature of approximately 0.4 °C and 0.8 °C at 14:00 LT for the modest and robust green increase scenario, respectively. The urban-rural energy surplus for cooling buildings is reduced and even counterbalanced. Peak CDHs decrease from 143 °C·h of the control case to 135 °C·h (modest increase) and 126 °C·h (robust increase), while they measure 137 °C·h in the non-urban areas. Average wind speed increases by 0.8 m/s (equal to 22 % with respect to the control case). Furthermore, adding urban greenery has an unfavorable implication on VC (maximum reduction of 500 m^2s^{-1}) with a consequent deterioration of the transport and dispersion of pollutants. Middle- and high-density classes are touched more than low-density by the VC reduction. In addition, the benefits of enhancing urban greenery concern physiologically and psychologically the quality of life of the dwellers.

1. Introduction

Consistently with Wilson's hypothesis about the natural feeling of human beings towards all living species (Wilson, 1992), a greater awareness is experiencing on the significance of expanding green spaces in cities to offer dwellers outdoor recreational opportunities (Balany et al., 2020; Krayenhoff et al., 2021). The benefits of contact with nature concern multiple aspects of the life of citizens, both from a physiological and psychological point of view (Klingberg et al., 2017; Diener and Mudu, 2021). Great emphasis is given to the urban greenery also for its thermal mitigation potential of the built environment, that is affected by the Urban Heat Island (UHI) and that will be additionally stressed by the global temperature rise expected until the end of the century (IPCC, 2023).

The Urban Heat Island (UHI) is defined as the temperature rise of the city in comparison with the surrounding rural zones (Akbari et al., 2015). The phenomenon depends on the synergic effect of difference sources: the reduction of green areas with consequent reduction of the surface permeability and evapotranspiration rate, the replacement of permeable surfaces with urban fabrics. The small sky view factor observed in densely constructed areas with high rise buildings is another cause for UHI, as the heat remains entrapped below the canopy layer (Dirksen et al., 2019).

The impacts and hazards due to urban overheating are observed at several levels: increment of energy uses for cooling, poor thermal comfort conditions in not cooled buildings, performance losses of energy systems (Santamouris, 2020). High temperatures also affect the thermoregulation on the human body, causing morbidity and mortality risks (Schinasi et al., 2018).

The above framework calls for an urgent mitigation of the urban built environment. Several well tested solutions are available to the purpose in addition to greenness (e.g., advanced materials and blue technologies), as illustrated by Lai et al. (2019).

Cooling the surrounding air by evapotranspiration is a well-known mechanism, especially during heat waves (HW) (Shiflett et al., 2017). This potential depends on several parameters such as the climate, the physical characteristics of the canopy, the geometry, and the morphology of the area (Klein and Coffman, 2015; Lynn and Lynn, 2020).

Two main approaches can be identified to assess the impact of urban greenery in cities: the simulation and the observation-based ones, which can be eventually integrated to support each other. The former includes both numerical and virtual techniques, while the last one relies on data collected in field and satellite products (Chen et al., 2014; Wang et al., 2022a, 2022b). It has been emphasized that empirical findings are constrained to highly specific cases (Bowler et al., 2010), while "what-if" scenarios such as those performed in this study are much more flexible, as well as able to parameterize the analysis and generalize the results.

Assessing the impact of green areas on the urban thermal environment by numerical analyses require big computational resources, and reliable and validated tools. The state-of-the-art Weather Research and Forecasting (WRF) has been widely used for UHI studies in recent years, as reported in the review paper by Zhu and Ooka (2023), as it also allows to reproduce "what-if" scenarios simulating the implementation of different mitigation techniques (e.g., Wang et al., 2022a, 2022b). Lots of WRF studies investigated the effects of expanded vegetated extents in cities in different climatic and geographical areas of the world, focusing on selected topics such as UHI and thermal comfort (Arghavani et al., 2020; Berardi et al., 2020; Li and Norford, 2016; Mughal et al., 2020; Khan et al., 2022). In such applications a key role is played by physical parameterizations in WRF, such as the Planetary Boundary Layer (PBL) schemes and the urban schemes. For both categories several options are available and a large literature is focused on the study of the influence of different parameterizations on WRF results in the urban context (Falasca and Curci, 2018; Segura et al., 2021; Wang and Hu, 2020; Bilang et al., 2022; Sussman et al., 2024). Urban schemes have been introduced as an alternative to bulk urban parameterization. The Single Layer Urban Canopy Model (SLUCM) was developed in the early 2000s by Kusaka et al. (2001) and Kusaka and Kimura (2004) and represents the first stage of complexity following the bulk model. Then, the Building Effect Parameterization (BEP Martilli et al., 2002) represents a further advance in complexity in the exchanges between buildings and the atmosphere. As for SLUCM, BEP considers shadowing, reflections, and trapping of shortwave and longwave radiation in street canyons with a 3D urban geometry. However, thanks to a multi-layer approach, BEP vertically distributes sources and sinks of heat, moisture, and momentum across the urban canopy layer. Furthermore, it models effects of walls, streets and roofs on momentum, turbulent kinetic energy, and potential temperature. A sketch of the differences between SLUCM and BEP/BEM is provided in Chen et al. (2011). Some constraints exist in the coupling between urban schemes and PBL schemes in WRF. In particular, the Bougeault-Lacarrere (Bougeault and Lacarrere, 1989) and Mellor–Yamada–Janjic (Janjic, 1994) PBL schemes are more widely coupled and tested with multi-layer schemes. They are both local schemes with a 1.5 order closure of the turbulent kinetic energy prognostic equation and the first one presents a non-local counter gradient term for convective conditions. Furthermore, the Bougeault-Lacarrere scheme has been specifically designed for BEP. For further details on the features of the PBL schemes embedded in WRF the reader is referred to the technical notes of WRF (Skamarock et al., 2019).

Although the influence of UHI on local atmospheric dynamics has been widely proved (e.g., Falasca et al., 2013) the implications of extended vegetated areas on circulation conditions and on cooling energy needs of buildings is not examined in the current literature. Furthermore, many studies generally target specific short periods, such as the HWs, when the thermal stressful conditions are the highest at city level. If this approach provides relevant results under the extreme, few data at seasonal scale are available which could provide more robust statistical basis to assess the impact of urban greenery. These are significant research gaps, together with the dichotomy between long observation analyses at low spatial resolution (e.g., Khan et al., 2022) and short analysis periods with high spatial resolution (e.g., Berardi et al., 2020).

Given the research gaps listed above, the goal of this article is thus assessing the impact of the progressive amplification of the urban green fraction on the urban environment considering features that have been

little or no explored to date, namely the ventilation coefficient and the cooling degree hours. To this end, an innovative configuration that combines the long simulation period with a high spatial resolution is used. A detailed description of the Methodology is provided in Section 2, while Results are displayed and discussed in Section 3 and 4, respectively. Conclusions are included in Section 5.

2. Methodology

2.1. Study area and period

Melbourne, capital of Victoria State, is the second most populous city in Australia with 5 million of inhabitants. Its urban and metropolitan ("Greater Melbourne") areas cover about 2.450 km^2 and 10,000 km^2, respectively. Melbourne is located on the southeastern coast of Australia and is characterized by a temperate oceanic climate with warm to hot summers and mild winters belonging to the Cfb class of the Koppen-Geiger classification (Beck et al., 2018). Due to its position, it is also affected by the sea-land breeze circulation with winds from the sea during the daytime.

In this study, the Australian summer months of January and February 2019, one of the warmest years for Australia (Bureau of Meteorology - BoM, 2016) were selected for the WRF runs.

2.2. Setup of the Weather Research and Forecasting (WRF) model

The WRF domain configuration has been designed to simulate weather variables in the atmospheric boundary layer over the city of Melbourne (Australia) at 500 m spatial resolution. The following four two-way nested domains have been defined with an increasing horizontal resolution (Fig. 1): i) domain d01, the largest one, covering the South-East of Australia (grid size equal to 13.5 km), ii) domain d02 (grid size equal to 4.5 km), iii) domain d03 (grid size equal to 1.5 km), iv) domain d04 covering the urban area of Melbourne (grid size equal to 0.5 km). The vertical grid presents 33 vertical levels with the lowest one at 12 m from the ground. The numerical setup consists of: the revised MM5 surface layer scheme, the Noah Land Surface Model, the Bougeault-Lacarrère Planetary Boundary Layer scheme, the multi-layer Building Effect Parameterization scheme (BEP - Martilli et al., 2002), the WRF Single-Moment 6-class scheme for microphysics, the RRTM and the Dudhia schemes for long wave and short wave respectively. For a detailed description of the listed physics option the reader is referred to the WRF user's guide (https://www2.mmm.ucar.edu/wrf/users/docs/user_guide_v4/v4.3/contents.html) and the technical notes (Skamarock et al., 2019). The numerical configuration has been designed based on previous similar studies and the comparison between the numerical results of preliminary tests and observations. Specifically, numerical experiments were carried out using different urban schemes and PBL schemes (i.e., Bougeault-Lacarrere- BouLac and Mellor-Yamada-Janic), a higher vertical resolution with up to 57 eta vertical levels. The selected configuration presents good performances (see Section 3.1) and reasonable time requirements, given the long period simulated. Initial and boundary conditions are the final operational global analysis data of the National Center for Environmental Prediction with spatial resolution of 0.25° × 0.25° and a temporal resolution of 6 h (NCEP, 2015). The spin-up period for each run is 12 h, not included in the analysis of results. Land use classification is provided by the MODIS dataset non-urban cells, and by the World Urban Database (Section 2.2.1) for the urban cells.

2.2.1. Urban land use

The urban land cover integrates the LCZ classification developed by Stewart and Oke (2012), following the community-based project called World Urban Database and Access Portal Tools project (https://www.wudapt.org/) (Ching et al., 2018). The LCZ classification consists in 17 urban zone types for a much more detailed representation of the urban texture, conveniently translated for WRF runs (Demuzere et al., 2022). The LCZ-based approach has been already employed for several cities (e.g., Barcelona (Ribeiro et al., 2021), Hong Kong (Du et al., 2022), Mumbai (Patel et al., 2020), San Jose (McRae et al., 2020), Singapore (Mughal et al., 2019)). Fig. 1b shows the land use categories present in the Melbourne setting, with urban categories corresponding to number equal and >31. In the following, data are grouped into three categories of urban density based on the urban land use, namely: i) Low Density (LD) including Heavy Industry and Sparsely Built, ii) Middle Density (MD) including Open High-Rise, Open Mid-Rise, Open Low-Rise, Large Low-Rise, iii) High Density (HD) including Compact High-Rise, Mid-Rise and Low-Rise. For a detailed description of the LCZs the reader is referred to Stewart and Oke (2012). In all three classes HD, MD and LD, each urban cell presents a percentage of surface area characterized by a green cover modeled as "cultivated/natural vegetation", the so-called urban green percentage. Non-urban cells count different vegetation types based on the MODIS dataset. However, since the differentiation between these vegetation types is not considered in this study, they are all categorized into a single "non-urban" group (Fig. 1b).

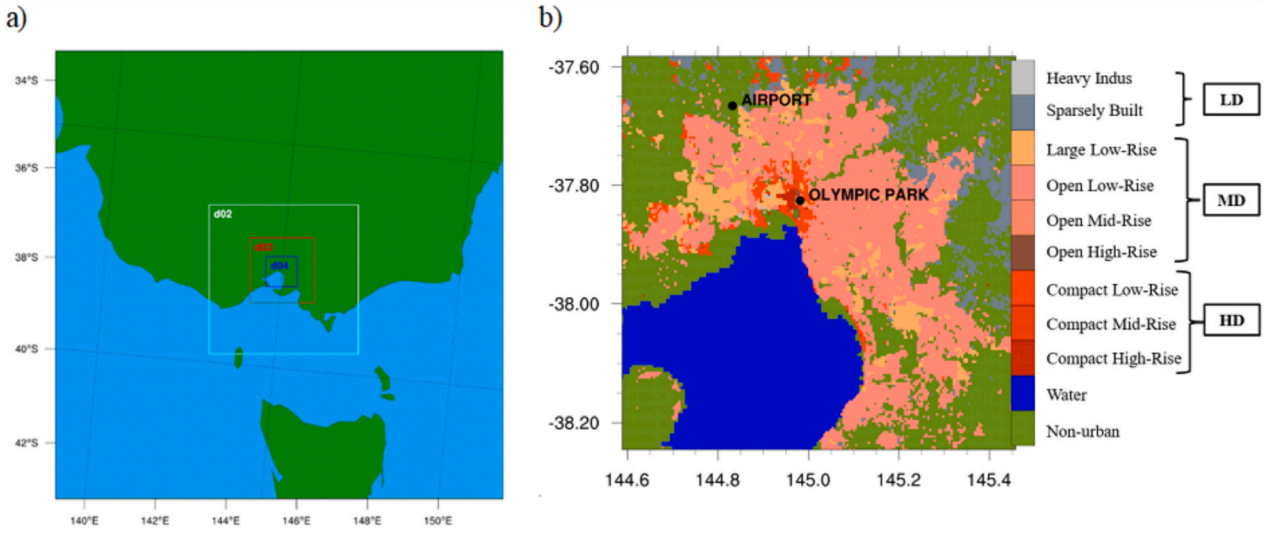


Fig. 1. a) Geographical areas covered by the four domains in the WRF runs; b) land use categories according to the LCZ classification in innermost domains (d04 in panel a). Urban categories are grouped in three categories, that is Low Density (LD), Middle Density (MD), High Density (HD).

2.3. Control case and urban green scenarios

In this work, a control case (CTRL) and two "what-if" scenarios with a progressive expansion of the average urban green fraction equal to 15 %, namely a modest increase scenario and a robust increase scenario, are numerically simulated (Table 1). The control case is characterized by an average percentage of urban greenery equal to 35 % due to the varied composition of LCZs (Section 2.2). Then, the modest increase scenario is characterized by an average urban green fraction equal to 50 % and the robust increase scenario is characterized by an average urban green fraction equal to 65 %. Such percentages have been computed through the weighted average of the urban green fractions of each density class considering the number of cells. The "what-if" scenarios have been obtained with a progressive amplification of the urban green fraction (modeled as "cropland/natural vegetation") of MD and HD classes while keeping that of the LD constant. More specifically, an equal increase in the urban greenery fraction has been applied to the MD and HD classes to obtain the average value desired. The fraction of urban greenery in LD has not been altered as the default value was higher than the average value for the entire city (35 %).

2.4. Data processing

2.4.1. Ventilation coefficient

The ventilation coefficient (VC) is defined as the product of the height of the planetary boundary layer (PBLH) and the wind speed (Saha et al., 2019):

$$VC = PBLH*WS \quad (1)$$

where PBLH is in [m] and WS the wind speed [m/s] averaged along the vertical direction from the ground to the PBLH. The Planetary Boundary Layer (PBL) is the part of the troposphere directly influenced by the Earth's surface (Stull, 1988). Surface forcings include, for example, mechanical drag, evapotranspiration, heat transfer and influence the PBL depth (PBLH). Within the PBL, pollutants and other quantities such as moisture are transported by the wind (WS) along the horizontal and by turbulence in the vertical. Thus, WS and PBLH are both crucial for the local air quality, the first governing the transport and the latter the dilution. VC combines these two quantities in a single parameter that quantify the air pollution potential over a region.

The conceptualization of VC dates back to the 20th century thanks to Holzworth (1967) and the idea was subsequently adopted and applied by several authors. Srivastava et al. (2010) interpreted the VC as "the rate by which pollutants within the mixed layer will be blown off from its location" and according to Genc et al. (2010) VC "is expected to provide more reliable information on the contribution of meteorology on air quality than both wind speed and mixing height alone". Nowadays, VC is commonly considered "as one of the factors determining pollution potential over a region of interest" (Lu et al., 2012). From a geographical point of view, VC applications mainly concern locations in the Asian continent. In terms of topics, some studies focus on the characterization of VC in different seasons and during the daily cycle (Gani et al., 2019; Shukla et al., 2022; Liu et al., 2019; Sun et al., 2023), while others focus on the relationship between pollutant levels and VC, all agreeing on the concomitance of poor air quality and low VCs (e.g., Srivastava et al., 2010; Hou et al., 2018).

Table 1
Features of the control case and of the urban green scenarios.

Case	Label	Average green fraction (%)
Control	CTRL	35
Average urban green equal to 50 % (modest increase)	gr50	50
Average urban green equal to 65 % (robust increase)	gr65	65

2.4.2. Cooling Degree Hours

The effects of the expansion of the urban greenery on the energy consumption for cooling the buildings is investigated though the Cooling Degree Hours (CDHs). CDHs are a proxy variable of the energy demand of for cooling a building and are computed as the cumulative sum of the positive differences between the external temperature and the setpoint temperature of the air conditioning systems (Salata et al., 2023). Such definition reads as in Eq. (2):

$$CDH = \sum_{h=1}^{n} (T_a - T_s)^+ \quad (2)$$

where T_a is the outdoor temperature [°C] and T_s is the set point temperature equal to 26 °C for residential buildings. The ASHRAE suggests set points in the 20–27 °C range for active cooling system. Australia does not have mandatory rules on the topic but just recommendation to use 25 °C. In the framework of decarbonization of the building stock, the setpoint for cooling is 26 °C by the Italian law and other (UNI, 2014). The outdoor temperature is reproduced by WRF at 2 m height with an hourly frequency. To date, applications of CDHs essentially concerns research on the impact of climate change (therefore with broader spatial and temporal resolutions than this study), where the future growth in cooling energy needs is evidenced (e.g., Livada et al., 2021; Shi et al., 2021).

3. Results

In this section results are displayed in terms of: i) weather variables describing the climate in the urban area of Melbourne such as air temperature at 2 m height and wind speed intensity at 10 m height, ii) ventilation coefficient (VC), influencing the pollutant dispersion, iii) CDHs as proxy variable of the energy consumptions. The effects on the relative humidity are examined in the Supplementary Material.

3.1. Evaluation of the model performance

The performance of WRF in simulating air temperature at 2 m and wind speed at 10 m in the control case is evaluated against data recorded by weather stations at Melbourne Airport (sparsely built land use category) and Olympic Park (low-rise land use category) for the January–February 2019 timespan simulated. The temperature diagnostic at 2 m provided by WRF takes into account the atmospheric stability regime in the surface layer and it is not obtained by interpolation of the temperature vertical profile The indices used to quantify these performances (Table 2) are the Mean and Fractional Bias (MB and FB), the Pearson correlation coefficient (r), the normalized mean square error (NMSE), the fraction of predictions within a factor of two of observations (FAC2). Definitions of these statistical parameters are given in the Supplementary Material (Section 1). In agreement with other WRF studies on Melbourne and other cities, the performance of the 2 m temperature simulation is better than that of the 10 m wind speed even if MB and FB are good also for 10 m wind speed at the Olympic Park station. In this case, the temperature simulation is satisfying with R equal to 0.94 and

Table 2
Statistical summary of the comparison of WRF simulations and observations at the Melbourne Airport and Olympic Park weather stations.

Statistical parameter	Airport		Olympic Park	
	T2	WS10	T2	WS10
Mean Bias (MB)	−0.063	−0.93	−0.45	0.055
Fractional Bias (FB)	−0.00084	−0.19	−0.019	0.022
Correlation Coefficient (R)	0.95	0.71	0.94	0.68
Normalized Mean Square Error (NMSE)	0.0083	0.19	0.0081	0.20
Fraction of predictions within a factor of two of observations (FAC2)	0.99	0.82	0.99	0.76

0.95 at the Olympic Park and Airport station, respectively, FAQ2 equal to 0.99 and NMSE of approximately 0.0080 (Table 2).

3.2. Description of the control case

Time series of the temperature at 2 m height for the CTRL case are provided in the Supplementary materials (Fig. 1S). Fig. 2a shows that the average daily air temperature (at 2 m height) extends from 18 °C in the early morning hours to 26 °C in the central hours of the day with slight differences among the different classes of urban density. LD has a minimum value marginally lower than the others, while HD reaches a maximum temperature value lower than that of the other classes (probably due to the shading of the buildings).

Fig. 3 highlights the thermal surplus of the urban area compared to the surrounding non-urban areas, with an average difference of 1.8 °C at 06:00 LT. The spatial distribution of temperatures is quite different at 14:00 LT, when the wind speed in higher than in the morning and is directed towards the city (due to the sea breeze), relieving urban thermal excess in the areas close to the coast (Fig. 3c). As described above, previous WRF articles on Melbourne have focused on a single HW or a series of HWs. This entails that reported air temperatures (often up to and above 40 °C) and UHI are higher than those reported in the present work. However, results agree on the increasing trend of hourly UHI values from day to evening (Imran et al., 2018, 2019).

The average wind speed (and, similarly, MD and HD) present values between 2 m/s (nighttime) and 3.5 m/s (daytime). LD is windier than the other classes throughout the day, with peaks of about 4 m/s (Fig. 2b) because of the reduced drag effect of the constructions (Rajeswari et al., 2022). Such wind speed levels fall in the "Light Breeze" (6–11 km/h) and "Gentle breeze" (12–19 km/h) categories of the empirical Beaufort wind force scale. Unlike ambient temperature, the spatial distribution of wind speed does not depend on the time of day, although with higher levels reached at 14:00 LT than at 06:00 LT (Fig. 3b and d). Indeed, both in the morning and in the early afternoon, the urban area is less windy than the surroundings, with the windiest area at northwest of the domain.

Being the product of PBLH and wind speed, the daily cycle of VC (Fig. 4) depends on those of the two factors. It reflects the trend of PBLH and WS (not shown here) that reach peaks values in the central hours of the day, respectively at 14:00 LT and 17:00 LT. Indeed, PBLH is controlled by the surface thermal forcing, more intense in the central hours of the day. Differences between the three urban density classes are not significant in this time slot, with LD having slightly higher values and HD slight lower values. In more detail, LD reaches VC levels close to 5400 m^2s^{-1} at 16:00 LT. At this same time, MD exhibits VC levels slightly above 5200 m^2s^{-1}, while HD levels do not reach 5000 m^2s^{-1}. During the evening and the night, all density classes present VC values close to 1000 m^2s^{-1}, that is a value high enough to guarantee good dispersion potential (Aravind et al., 2022). Unlike daytime, LD presents lower VC than the other classes. VC levels simulated in this study are congruent with those simulated for the Indian coastal city of Chennai (i.e., Rajeswari et al., 2022).

Fig. 5 displays CDH levels at each hour of the day averaged over all the cells characterized by urban land use, regardless of the density class. An analogous representation has been realized for the single density class, but it is not shown in the article as it is not meaningful. The daily evolution of CDHs (Fig. 5) follows that of the 2 m temperature (Fig. 2). Indeed, it is reasonable that the setpoint temperature is exceeded mainly in the central hours of the day with a substantial contribution to the CDHs. Maximum levels of urban CDHs are just over 140 °C·h. As expected, CDHs are predominantly higher in urban than in non-urban areas due to the UHI. And for the same reason, the delta between urban and non-urban CDHs is higher during the night than during the day. The spatial distribution of the CDHs (not shown here) is comparable to that of the 2 m temperature both at 06:00 LT and 14:00 LT (Fig. 3). Considering the individual density classes, LD has the lowest total value (1200 °C·h), while MD and HD 1208 °C·h and 1210 °C·h, respectively. The average total value for the non-urban area is equal to 1105 °C·h (Table 3).

3.3. Description of the impact of greenery increase

3.3.1. Effects on temperature and CDHs

Timeseries of the 2 m temperature difference between the two scenarios gr50 and gr65 and the CTRL case are displayed in the Supplementary material (Fig. 2S) for the entire simulated period and the three density classes. The raise in the percentage of urban greenery in the two scenarios causes a progressive abatement in the 2 m temperature (Fig. 6 and Fig. 7). Such decrease slightly affects also regions bordering the urban area and characterized by non-urban land use. This phenomenon is especially evident at 14:00 LT (Fig. 6) and is attributable to the effect of the sea breeze, as also observed in the case of the application of high albedo materials (Falasca et al., 2022). From the point of view of the daily cycle of the temperature drop (Fig. 7), MD ranges between 0.2 °C (in the evening and at night) and about 0.4 °C at 14:00 in the modest increase scenario (gr50) and between 0.4 °C and 0.8 °C in the robust increase scenario (gr65). HD and LD present close temperature drops lower than the MD and reach a maximum value of about 0.2 °C in g50 and between 0.4 °C and 0.6 °C in gr65. Since the average daily temperatures of the three classes LD, MD and HD are comparable, this means that the relative impact is also higher in MD. Furthermore, it is remarkable that 2 m temperature diminishes also in LD where the urban green percentage is not altered. Given that the peak temperature decrease reaches nearly 1.5 °C in the highest albedo scenario (Falasca et al., 2022), the thermal drop calculated here (always lower than 1 °C) does not appear significant even in gr65. Nevertheless, from an energy point of view, the gr50 and gr65 show noteworthy improvements.

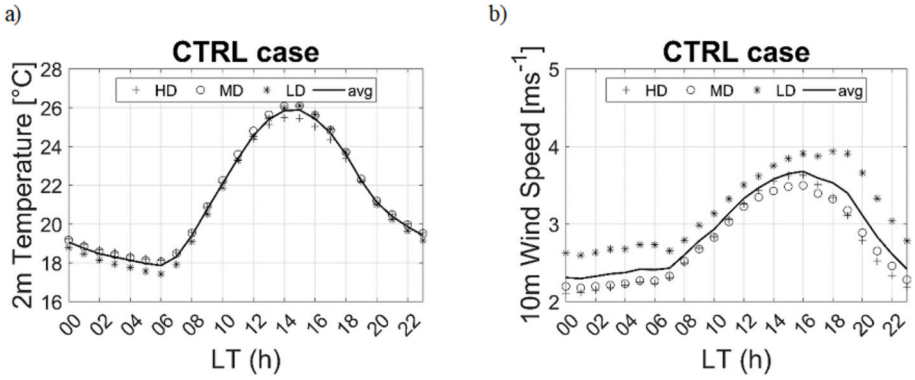


Fig. 2. Daily cycles of (a) temperature at 2 m height and (b) wind speed at 10 m height. Urban land categories are Low Density (LD), Middle Density (MD), High Density (HD), all density (avg).

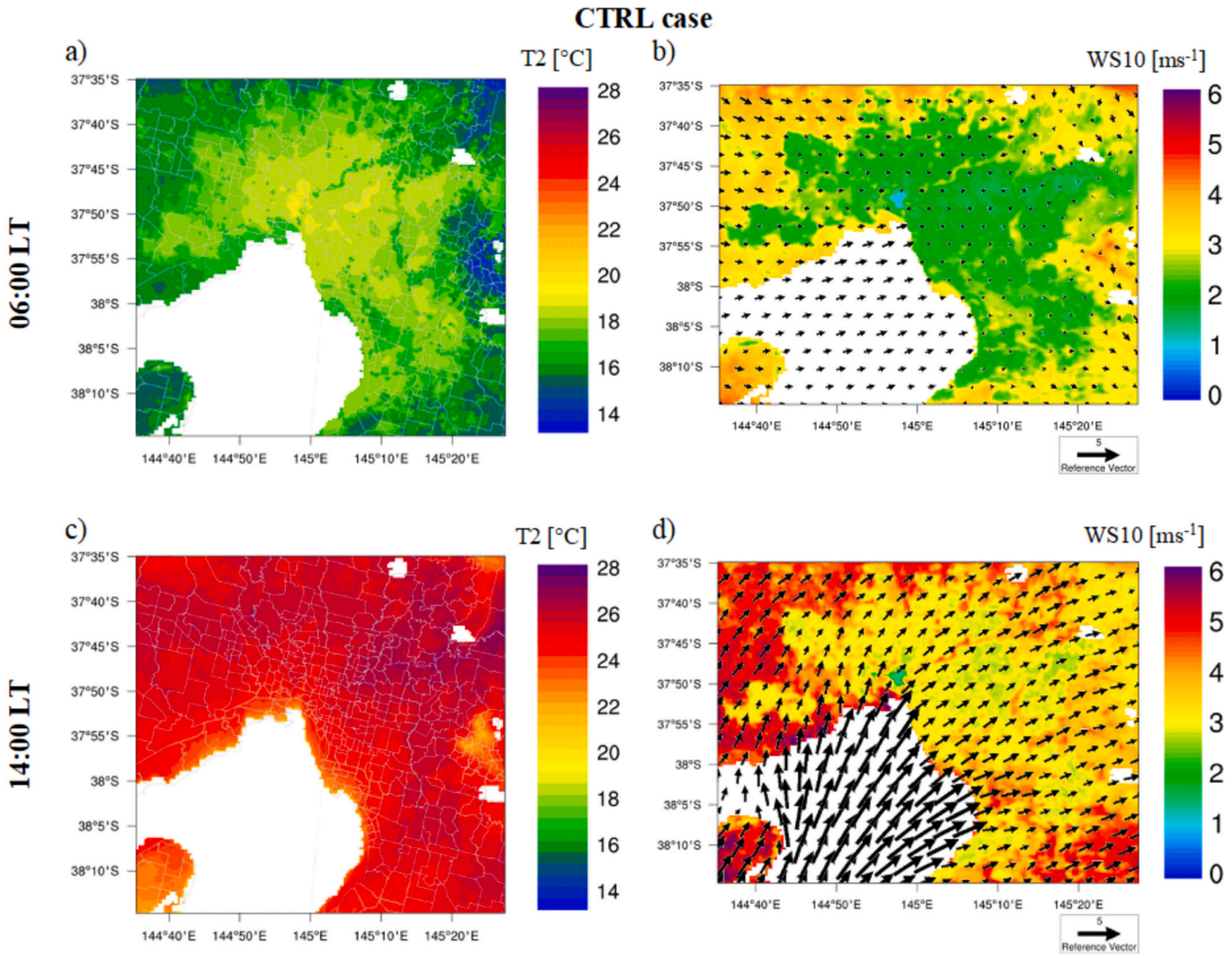


Fig. 3. Spatial distribution of temperature at 2 m height and wind speed at 10 m height and vectors in the innermost domain at 06:00 LT (a, b) and at 14:00 LT (c, d).

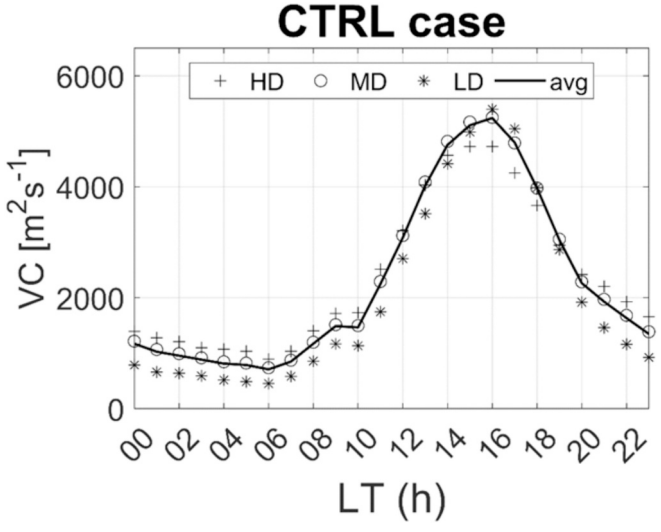


Fig. 4. Daily cycle of the ventilation coefficient (VC) in the CTRL case. Urban land categories are Low Density (LD), Middle Density (MD), High Density (HD), all density (avg).

Temperature is the unique variable involved in the calculation of the CDHs (Eq. (2)), therefore their alteration in the gr50 and gr65 scenarios is a direct consequence of the temperature modification. In both scenarios (gr50 and gr65) the spatial distribution of CDHs levels is essentially similar to that of the CTRL case, albeit with lower values thanks to the urban green enhancement. The highest CDH levels are still located north-east of the domain and the lowest levels nearby the sea (not shown here). Fig. 8 shows the average hourly values of urban CDHs for the CTRL case and the two scenarios gr50 and gr65 together with those of the non-urban areas in the CTRL run. Based on what has been observed for the temperature, it is reasonable to recognize that the difference between the scenarios and the CTRL case is negligible at night and noteworthy during the central hours of the day, especially for gr65. Clearly, the slight night-time drop in temperature is not enough to influence the difference between the ambient temperature and the set-point temperature. Moreover, during the night urban CDHs are always higher than non-urban ones. During the day, on the other hand, the CDH drops in the gr50 scenario (136 °C·h) to values very close to the non-urban ones (137 °C·h) and are even lower than the latter in the gr65 scenario (127 °C·h).

Finally, Table 4 lists the amounts of CDHs in the three simulated cases and for each of the three urban density classes. Such quantities look very close for each case, however in the two scenarios it is possible to calculate a difference of about 4 % (gr50) and 8 % (gr65) against the

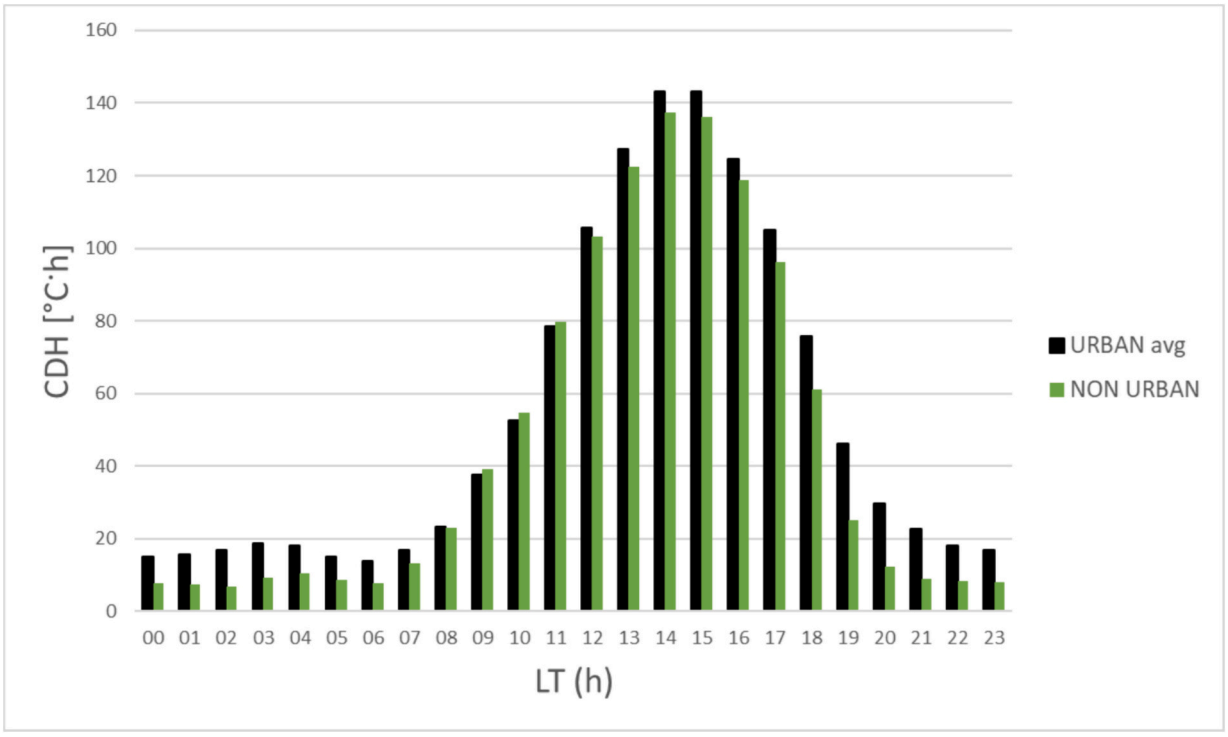


Fig. 5. Average hourly levels of CDHs in the CTRL case.

Table 3
Total CDHs for each density class.

Density class	CDH [°C·h]
HD	1210
MD	1208
LD	1200
Non-urban	1105

CTRL case.

3.3.2. Effects on wind speed intensity and ventilation coefficient

The expansion of the urban green mainly determines an intensification of 10 m wind speed, even if not in all districts (Fig. 9), contrary to what happens with the temperature. Indeed, the replacement of built surfaces with vegetation in gr50 and gr65 scenarios affects 10 m wind speed in MD, where the number of cells involved in the alteration of the in green fraction is meaningful. In LD and HD, the 10 m wind speed modification is essentially negligible as the first category is not involved in the enhancement of urban greenery and the latter one has a limited number of cells involved. On the other hand, MD presents 10 m wind speed differences up to 0.6 m/s in gr65 (Fig. 10). This is consistent with the fact that LD is windier than the other two classes in the reference case (Fig. 2b) due to the lack of obstacles limiting the near surface wind speed. It is worth pointing out that the effect of the vegetation expansion on wind intensity has a highly local character, much more than for temperature and related variables (i.e., CDHs).

Wind speed in the PBL contributes to the transport of pollutants and, in this case, to the levels of VC together with PBLH. Fig. 11 displays the average daily variation of VC between the two scenarios and the CTRL case for the three density classes. A similar outcome can be observed for the three classes LD, MD, HD except for the magnitude of the differences. PBLH falls for the three classes in both scenarios (more in gr65, as expected) as it is linked to the surface thermal forcing, while the wind speed has an opposite behavior along the day, with an intensification during daytime. In both the gr50 and gr65 scenarios the VC decreases more in HD and MD than in LD; as regards the magnitude of the differences, in gr65 the peak differences reach and exceed 500 m^2s^{-1} for MD while they are around 470 m^2s^{-1} for LD, in gr50 they are about 240 m^2s^{-1} for MD and 220 m^2s^{-1} LD.

4. Discussion

In this section the overall significance of this research is discussed. Moreover, the comparison with other published papers allows to point out its original contribution together with its limitations.

4.1. Comparison with other WRF studies

Many numerical studies are published that analyze the impact of green infrastructure on the mitigation of the thermal urban environment both at mesoscale and microclimatic scale. In their review on the existing literature on the matter, Santamouris and Osmond (2020) highlighted its profound heterogeneity in the research questions, in the methodology and consequently in the results. Therefore, only a comparison between results achieved in the present research and some other analogous published article is possible, as done in the following. The main results are summarized focusing in particular on the temperature difference between the scenario with expanded greenery and the reference case, considering that the complexity of the software, the handling of initial land use and the green infrastructure application led to significant variations from case to case.

Examples of WRF studies focused on long periods such as continuative summer /winter months or even seasons exist, such as those by Macintyre and Heaviside (2019), Macintyre et al. (2021) and Khan et al. (2022), with a maximum horizontal resolution of 2 km (the first one) and 1 km (the latter two). However, literature on WRF exercises is mostly focused on (a sequence of) short periods, generally associated to specific extreme events as the heat wave (HW) (e.g., Imran et al., 2018; Liu and Morawska, 2020). In this context, the original feature of the present experiments is the combined simulation across a long summer period (2 months) with a high-resolution domain (0.5 km).

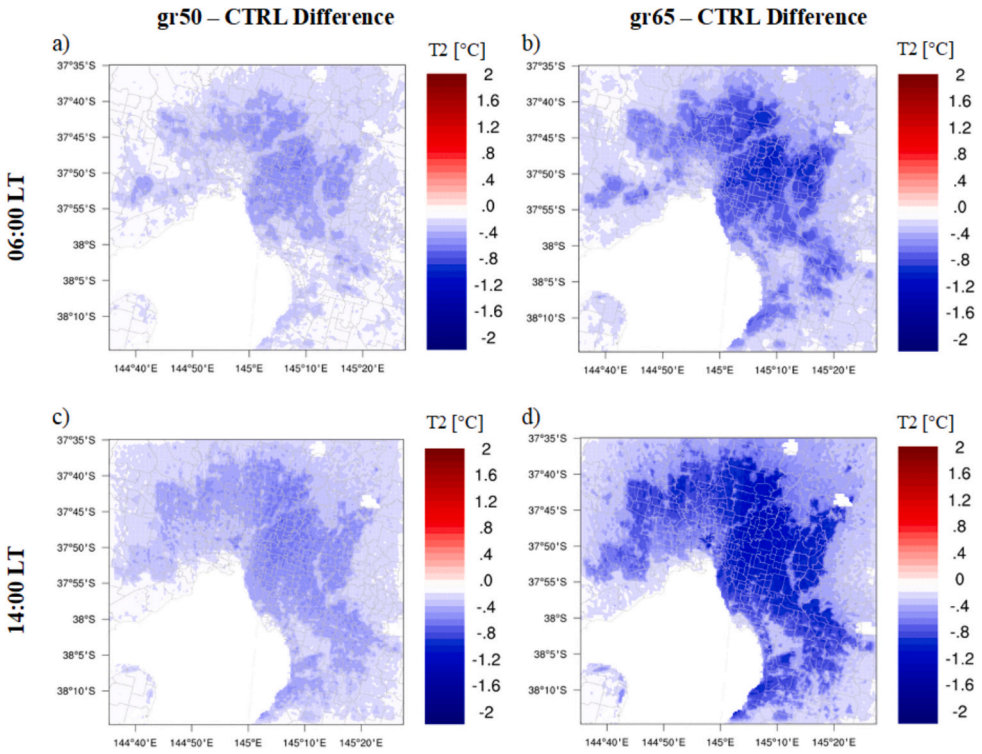


Fig. 6. Spatial distribution of the scenarios – reference case deviation for temperature at 2 m height at 06:00 LT and 14:00 LT for gr50 (a, c) and gr65 (b, d) scenarios.

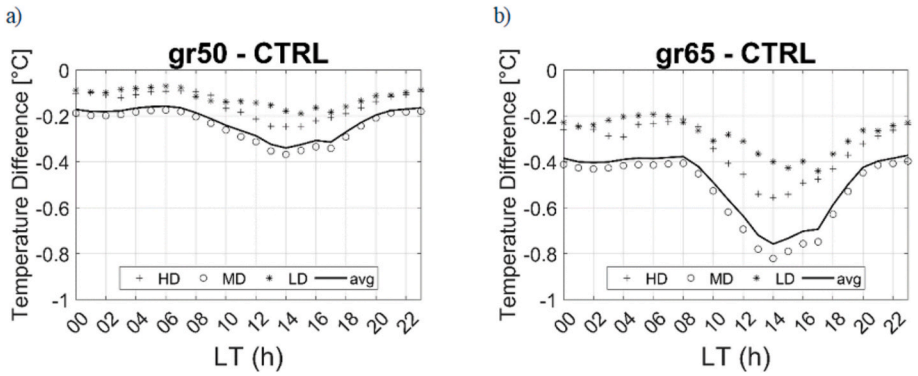


Fig. 7. Scenario-reference case deviation for temperature at 2 m height: a) modest increase scenario gr50, b) robust increase scenario gr65. Urban land categories are Low Density (LD), Middle Density (MD), High Density (HD), all density (avg).

The present investigation proves that peak values of the temperature drop averaged over all urban cells range from 0.4 to 0.8 °C at 14:00 in the gr50 and gr65 scenario, respectively. Berardi et al. (2020) carried out a similar study for Toronto (Canada) during a HW event and found a daily temperature drop ranging by 1.6 °C to 2.3 °C with a green coverage enlargement by 50 % and 80 %, respectively. Analyzing the impact of vegetation during a HW was the core of a study of Imran et al. (2019) for Melbourne (Australia) who simulated a progressive enlargement of greenness from 20 % to 50 %, considering a single urban built type, but different types of vegetation. They found a negligible daytime mitigation effect and a nighttime peak drop of 0.6 °C and 3.0–3.7 °C (as a function of the green species) for the 20 % and 50 % green fraction increase, respectively. Similar topic for the same city was studied in Jacobs et al. (2018) for 12 HWs in the 1990–2014 time span with three green scenarios consisting in increasing the vegetation fraction by 5, 10 and 40 % in the three (low, medium, high) density classes. The first two scenarios lead to negligible average daily temperature reductions, peaking 0.4 °C at nighttime for the 10 % increase of green fraction, while a 1 °C temperature drop was calculated for 40 % increase of green fraction at midnight as city average, with peak around 2.4 °C in some north and west zones of the city. An analogous approach with three density classes (low intensity residential, high-intensity residential, and industrial or commercial) was followed by Khan et al. (2022) for a WRF study on Athens, Greece. The green fraction was increased by 30, 50 and 70 % in the urban built areas, being 10 % in the initial configuration. The average temperature drop was 0.4, 0.7 and 1.0 °C for the three scenarios, respectively; also peak temperature reductions were higher at night than at daytime, being 1.9 °C and 1.2 °C, respectively. Mughal et al. (2020) found that in Singapore the air temperature diminishes by 0.5–1.6 °C through all day, but higher temperature drops were calculated during the night/early morning hours (1.3–1.6 °C), on the other side relative humidity increase by 8 % were calculated during the same hours, which is critical for a city where this parameter is seldom below 70 %.

Other thoughts pertain to the numerical configuration. The literature survey described above show that WRF studies on the topic agree that the expansion of urban greenery brings thermal benefits, but they

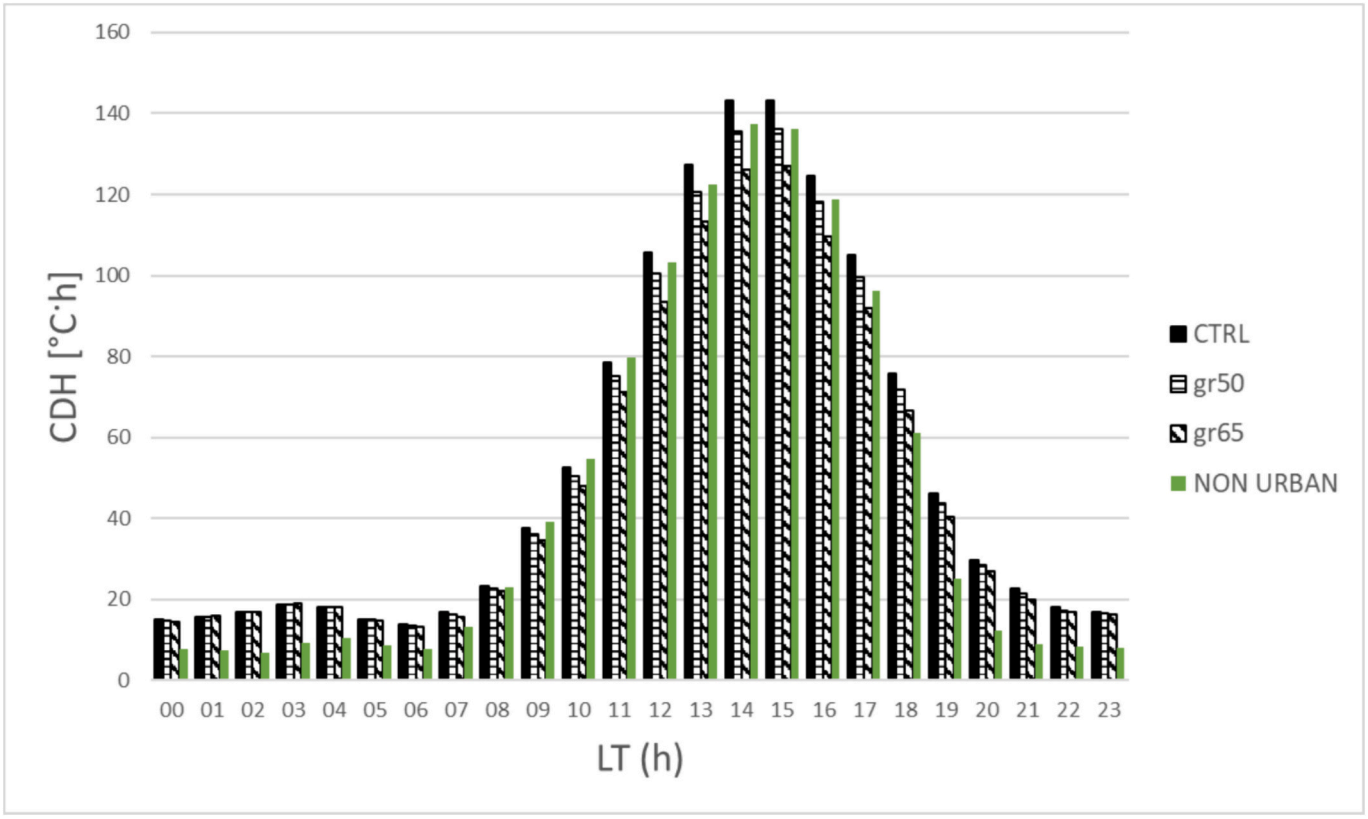


Fig. 8. Average hourly levels of CDHs in the CTRL case and in the two green increase scenarios.

Table 4
Total amount of CDHs in the different urban classes for each simulated case.

Case	High density [°C·h]	Middle density [°C·h]	Low density [°C·h]
CTRL	1210	1208	1200
gr50	1164	1161	1151
gr65	1113	1110	1103

disagree on the time of day of maximum benefit. Indeed, some of them (including the Single Layer Urban Canopy Model – SLUCM by Kusaka et al., 2001) predict a higher thermal benefit at night or in the early morning than in the central hours of the day, while other (including the multi-layer BEP and BEP-BEM, by Martilli et al., 2002 and Salamanca and Martilli, 2010) and the present research estimate a higher temperature fall in the central hours of the day. Additional tests holding all else equal (not shown here) demonstrate that such feature depends on the urban scheme. Experimental argumentations on this issue were sought in the literature. Hamada and Ohta (2010) detected higher daytime temperature differences between urban and green areas during their summertime measurement campaigns (Hamada and Ohta, 2010). Potchter et al. (2006) came to similar conclusions for parks with high and wide-canopied trees. Their and other surveys' results (e.g., Duncan et al., 2019) thus suggest that the cooling ability depends on several factors affecting humidity and radiation, first the vegetation type.

4.2. Strength and limitations

As discussed in the previous section, the WRF configuration used in this study has novel elements, such as the high resolution and the simulated two-month period. All this makes this tool important for the evaluation of the implications of increased urban greenery on energy and air circulation (in addition to the cooling potential), which have been little explored so far. It also provides statistically relevant data for the analysis of microclimatic changes due to modified green areas across the city. The length of the simulated period entailed some constraints in the numerical setup, such as the coarse vertical resolution. However, it was verified that this configuration did not significantly affect the results presented. The relevance of hypothetical settings and city-scale surveys for planning and policymaking is often emphasized (Herath et al., 2021). Results highlight the impact of geometric/morphologic factors on numerical results, as already established by numerous observational works (Santamouris and Osmond, 2020). The features of the simulated urban vegetation also influence the level of interaction of the vegetation with the lower atmospheric layers and therefore the results. In this study, this aspect was not explored given that only the cropland/natural vegetation class was considered in the "what-if" scenarios, characterized by a low roughness. Investigating the effect of vegetation type is fundamental, however at this stage it is beyond the scope of the present research, which is focused on the impact of increasing the extent of green surface. For this reason, the "what-if" scenarios vary compared to the reference case and among themselves only in the percentage of the green percentage. The lack of differentiation of vegetation species and patterns as well as the examination of their impact on the outcomes constitutes at this step the main limitation of this study.

5. Conclusions

This study explores the effects of increasing the urban green coverage in Melbourne from different perspectives, such as urban climate, air circulation and energy needs for cooling residential buildings. Its importance arises from the awareness of: i) the importance of exploring the potential of this mitigation technique in the context of climate change, given the projections of HWs rise both in intensity and frequency, ii) to better understand the outcomes of urban greenery that have been little explored up to now, namely about local air circulation and energy consumption for cooling buildings. To this end, a control

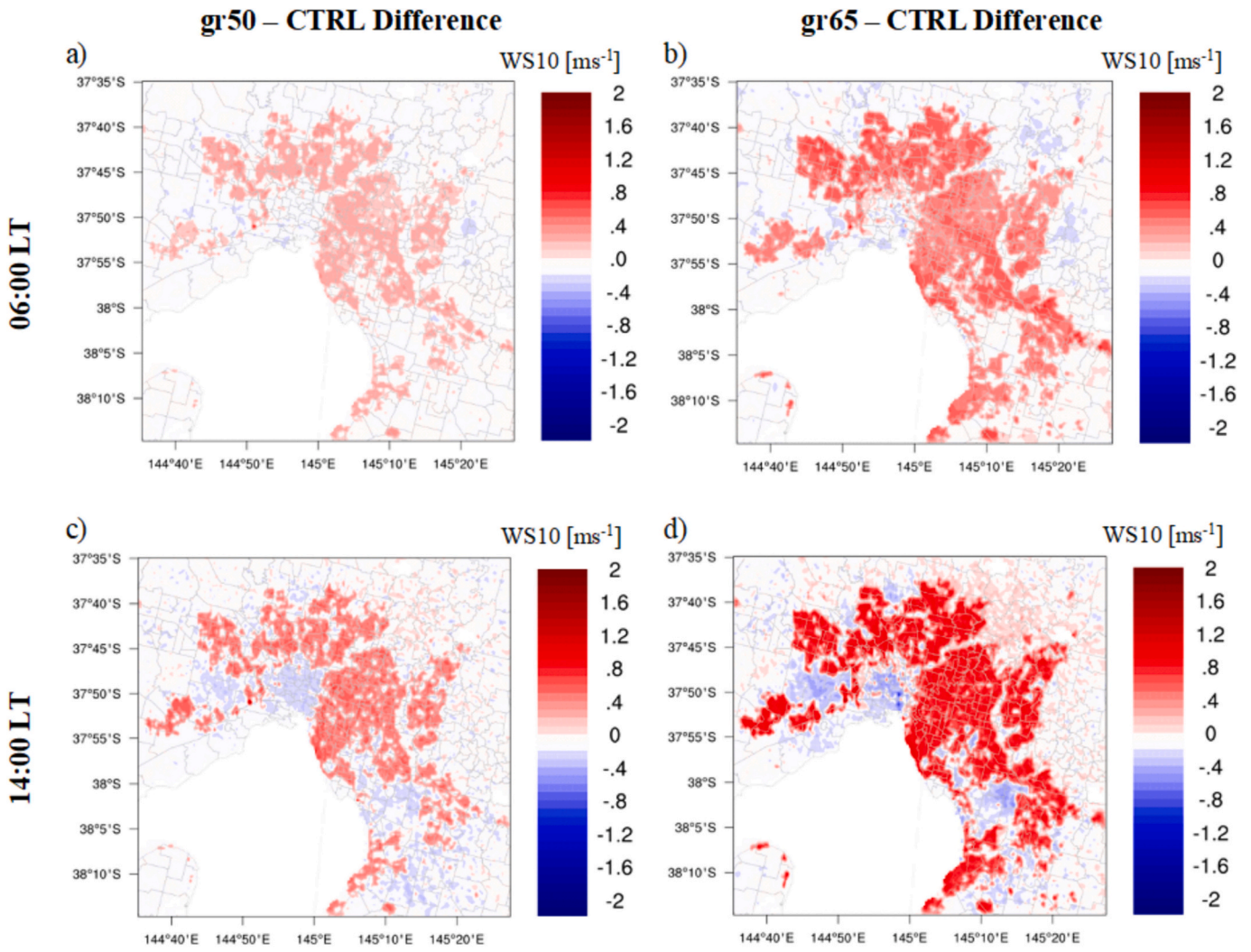


Fig. 9. Spatial distribution of the scenarios – reference case deviation for wind speed at 10 m height at 06:00 LT and 14:00 LT for gr50 (a, c) and gr65 (b, d) scenarios.

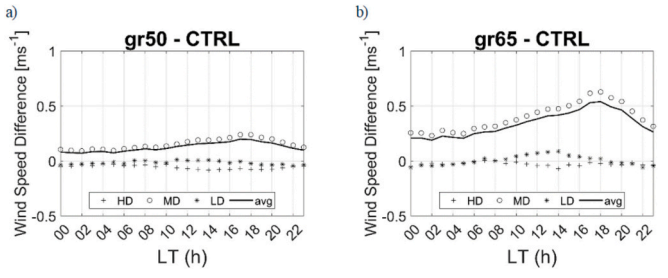


Fig. 10. Scenario-reference case deviation for wind speed at 10 m height: a) modest increase scenario gr50, b) robust increase scenario gr65. Urban land categories are Low Density (LD), Middle Density (MD), High Density (HD), all density (avg).

case and two "what-if" scenarios characterized by an urban coverage of 35 %, 50 % and 65 % have been simulated using a WRF configuration integrating the LCZ for the city of Melbourne. Since the focus of the work is the increase of the green surface in the city, the type of vegetation is kept constant (cropland/natural vegetation) in the three simulated cases. Then, two meteorological variables (temperature at 2 m height and wins speed at 10 m height), the ventilation coefficient and the cooling degree hours have been analyzed. Also results on relative humidity are illustrated in the Supplementary Material.

Melbourne is a temperate oceanic metropolis located in the northeast coast of Australia. The coastal position of the city means that the city is affected by the sea breeze with consequences both on the local climate and on the effects of the enlargement of urban greenery.

The state of the atmospheric layer in contact with the Earth's surface, the so-called PBL, is strongly influenced by surface thermal and mechanical forcings. UHI mitigation techniques impact both kinds of forcings, individually or together. In the case of the greenery enhancement, both types of forcing are affected at the same time because of the modification in the surface energy balance and the roughness, with consequences on local weather variables, such as near-surface temperature and wind speed and PBLH. Concerning the temperature at 2 m, maximum daily drop occurs in the MD class and is about 0.4 °C for gr50 and 0.8 °C for gr65. Such reduction is higher also in percentage for MD compared to the reference case. Correspondingly, there is a decrease in the CDH which leads them to equal and even fall below the non-urban CDH. It is crucial to consider that reducing the energy demand for cooling buildings not only saves money for people, but also saves fossil fuels that power electrical systems and consequently benefits the planet. Furthermore, the thermal drop in the two scenarios does not concern only the urban area where the green coverage has been enlarged, but also the adjacent non-urban areas located in the direction where the sea breeze blows. This phenomenon, also observed in a similar study on high albedo materials, is particularly evident in the hours of maximum sea breeze intensity.

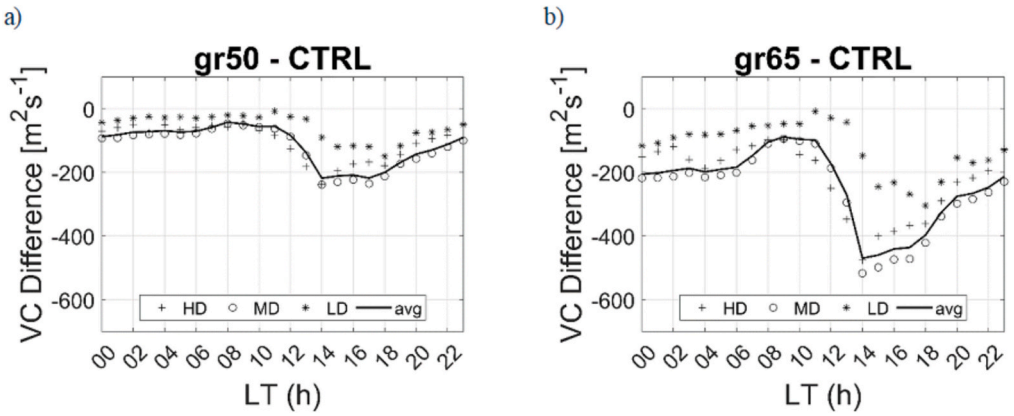


Fig. 11. Scenario-reference case deviation for ventilation coefficient: a) modest increase scenario gr50, b) robust increase scenario gr65. Urban land categories are Low Density (LD), Middle Density (MD), High Density (HD), all density (avg).

In this article, the ventilation coefficient has been adopted as an index quantifying the air pollution potential of the PBL, that is the product of PBLH and the average wind speed within the PBL. Indeed, PBLH and wind speed contribute individually to dilution and transport of scalars (e.g., pollutants) and together to ventilation. In general, the reduction of surface thermal forcings weakens buoyancy and thus the dilution of pollutants. In this study, given the vegetation type simulated (low vegetation), its expansion determines a decrease in roughness compared to the control case with a concomitant increase in wind speed. Overall, the increase in urban greenery determines an overall decrease in the VC with the associated worsening of the transport and dispersion of locally produced pollutants. This concerns all three urban classes, even if MD is touched more than HD and LD due to the reduced number of buildings in the highest number of cells.

These conclusions are necessarily bounded to the numerical setup applied, including the design of the numerical simulations. Based on the outcomes and remarks on the limitations of this work, its natural development in the future should be the exploration of the impact of the type of greenery introduced in the city for the purposes of mitigating UHI and HWs.

CRediT authorship contribution statement

Serena Falasca: Writing – original draft, Software, Methodology, Investigation, Formal analysis, Conceptualization. **Michele Zinzi:** Writing – original draft, Methodology, Investigation, Conceptualization. **Anna Maria Siani:** Writing – review & editing, Methodology, Conceptualization. **Gabriele Curci:** Writing – review & editing, Methodology, Formal analysis. **Lan Ding:** Writing – review & editing. **Mattheos Santamouris:** Writing – review & editing, Supervision, Conceptualization.

Declaration of competing interest

The authors declare that they have no known competing financial interests or personal relationships that could have appeared to influence the work reported in this paper.

Data availability

Data will be made available on request.

Acknowledgements

Serena Falasca gratefully acknowledges fellowship funding from MUR (Ministero dell'Università e della Ricerca) under PON "Ricerca e Innovazione" 2014-2020 (D.M. 1062/2021). This research was partially funded by "Progetti di Ricerca Grandi" of Sapienza University of Rome (Prot. RG123188AFDE2E0D). The computational resources for WRF runs were provided by CINECA and CRESCO/ENEAGRID High Performance Computing infrastructure. We acknowledge the CINECA award under the ISCRA initiative, for the availability of high-performance computing resources and support. The computing resources and the related technical support used for this work have been provided also by CRESCO/ENEAGRID High Performance Computing infrastructure and its staff (F. Iannone et al., "CRESCO ENEA HPC clusters: a working example of a multifabric GPFS Spectrum Scale layout," 2019 International Conference on High Performance Computing & Simulation (HPCS), Dublin, Ireland, 2019, pp. 1051-1052, https://doi.org/10.1109/HPCS48598.2019.9188135.). CRESCO/ENEAGRID High Performance Computing infrastructure is funded by ENEA, the Italian National Agency for New Technologies, Energy and Sustainable Economic Development and by Italian and European research programs, see http://www.cresco.enea.it/english for information.

Appendix A. Supplementary data

Supplementary data to this article can be found online at https://doi.org/10.1016/j.scitotenv.2024.176016.

References

Akbari, H., Cartalis, C., Kolokotsa, D., Muscio, A., Pisello, A.L., Rossi, F., Santamouris, M., Synnef, A., Wong, N.H., Zinzi, M., 2015. Local climate change and URBAN heat island mitigation techniques – the STATE of the art. J. Civ. Eng. Manag. 22, 1–16. https://doi.org/10.3846/13923730.2015.1111934.

Aravind, A., Srinivas, C.V., Hegde, M.N., Seshadri, H., Mohapatra, D.K., 2022. Impact of land surface processes on the simulation of sea breeze circulation and tritium dispersion over the Kaiga complex terrain region near west coast of India using the weather research and forecasting (WRF) model. Atmos. Environ. X 13, 100149. https://doi.org/10.1016/j.aeaoa.2022.100149.

Arghavani, S., Malakooti, H., Ali Akbari Bidokhti, A.-A., 2020. Numerical assessment of the urban green space scenarios on urban heat island and thermal comfort level in Tehran Metropolis. J. Clean. Prod. 261, 121183 https://doi.org/10.1016/j.jclepro.2020.121183.

Balany, F., Ng, A.W., Muttil, N., Muthukumaran, S., Wong, M.S., 2020. Green infrastructure as an urban Heat Island mitigation strategy—a review. Water 12, 3577. https://doi.org/10.3390/w12123577.

Beck, H.E., Zimmermann, N.E., McVicar, T.R., Vergopolan, N., Berg, A., Wood, E.F., 2018. Present and future Köppen-Geiger climate classification maps at 1-km resolution. Sci. Data 5, 180214. https://doi.org/10.1038/sdata.2018.214.

Berardi, U., Jandaghian, Z., Graham, J., 2020. Effects of greenery enhancements for the resilience to heat waves: a comparison of analysis performed through mesoscale (WRF) and microscale (Envi-met) modeling. Sci. Total Environ. 747, 141300 https://doi.org/10.1016/j.scitotenv.2020.141300.

Bilang, R.G.J.P., Blanco, A.C., Santos, J.A.S., Olaguera, L.M.P., 2022. Simulation of urban Heat Island during a high-heat event using WRF urban canopy models: a case study for metro Manila. Atmosphere 13, 1658. https://doi.org/10.3390/atmos13101658.

Bougeault, P., Lacarrere, P., 1989. Parameterization of orography-induced turbulence in a mesobeta–scale model. Mon. Weather Rev. 117, 1872–1890. https://doi.org/10.1175/1520-0493(1989)117<1872:POOITI>2.0.CO;2.

Bowler, D.E., Buyung-Ali, L., Knight, T.M., Pullin, A.S., 2010. Urban greening to cool towns and cities: a systematic review of the empirical evidence. Landsc. Urban Plan. 97, 147–155. https://doi.org/10.1016/j.landurbplan.2010.05.006.

Bureau of Meteorology (BoM), 2016. How will I know if a heatwave is coming?. Retrieved July 20, 2020, from How will I know if a heatwave is coming? website. http://media.bom.gov.au/social/blog/891/how-will-i-know-if-a-heatwave-is-coming/ (Last access 26th October 2023).

Chen, A., Yao, X.A., Sun, R., Chen, L., 2014. Effect of urban green patterns on surface urban cool islands and its seasonal variations. Urban For. Urban Green. 13, 646–654. https://doi.org/10.1016/j.ufug.2014.07.006.

Chen, F., Kusaka, H., Bornstein, R., Ching, J., Grimmond, C.S.B., Grossman-Clarke, S., Loridan, T., Manning, K.W., Martilli, A., Miao, S., Sailor, D., Salamanca, F.P., Taha, H., Tewari, M., Wang, X., Wyszogrodzki, A.A., Zhang, C., 2011. The integrated WRF/urban modelling system: development, evaluation, and applications to urban environmental problems. Int. J. Climatol. 31, 273–288. https://doi.org/10.1002/joc.2158.

Ching, J., Mills, G., Bechtel, B., See, L., Feddema, J., Wang, X., Ren, C., Brousse, O., Martilli, A., Neophytou, M., Mouzourides, P., Stewart, I., Hanna, A., Ng, E., Foley, M., Alexander, P., Aliaga, D., Niyogi, D., Shreevastava, A., Bhalachandran, P., Masson, V., Hidalgo, J., Fung, J., Andrade, M., Baklanov, A., Dai, W., Milcinski, G., Demuzere, M., Brunsell, N., Pesaresi, M., Miao, S., Mu, Q., Chen, F., Theeuwes, N., 2018. WUDAPT: an urban weather, climate, and environmental modeling infrastructure for the Anthropocene. Bull. Am. Meteorol. Soc. 99, 1907–1924. https://doi.org/10.1175/BAMS-D-16-0236.1.

Demuzere, M., Argüeso, D., Zonato, A., Kittner, J., 2022. W2W: a Python package that injects WUDAPT's local climate zone information in WRF. JOSS 7, 4432. https://doi.org/10.21105/joss.04432.

Diener, A., Mudu, P., 2021. How can vegetation protect us from air pollution? A critical review on green spaces' mitigation abilities for air-borne particles from a public health perspective - with implications for urban planning. Sci. Total Environ. 796, 148605 https://doi.org/10.1016/j.scitotenv.2021.148605.

Dirksen, M., Ronda, R.J., Theeuwes, N.E., Pagani, G.A., 2019. Sky view factor calculations and its application in urban heat island studies. Urban Clim. 30, 100498 https://doi.org/10.1016/j.uclim.2019.100498.

Du, R., Song, J., Huang, X., Wang, Q., Zhang, C., Brousse, O., Chan, P.W., 2022. High-resolution regional modeling of urban moisture island: mechanisms and implications on thermal comfort. Build. Environ. 207, 108542 https://doi.org/10.1016/j.buildenv.2021.108542.

Duncan, J.M.A., Boruff, B., Saunders, A., Sun, Q., Hurley, J., Amati, M., 2019. Turning down the heat: an enhanced understanding of the relationship between urban vegetation and surface temperature at the city scale. Sci. Total Environ. 656, 118–128. https://doi.org/10.1016/j.scitotenv.2018.11.223.

Falasca, S., Curci, G., 2018. High-resolution air quality modeling: sensitivity tests to horizontal resolution and urban canopy with WRF-CHIMERE. Atmos. Environ. 187, 241–254. https://doi.org/10.1016/j.atmosenv.2018.05.048.

Falasca, S., Moroni, M., Cenedese, A., 2013. Laboratory simulations of an urban heat island in a stratified atmospheric boundary layer. J. Vis. 16, 39–45. https://doi.org/10.1007/s12650-012-0150-1.

Falasca, S., Zinzi, M., Ding, L., Curci, G., Santamouris, M., 2022. On the mitigation potential of higher urban albedo in a temperate oceanic metropolis. Sustain. Cities Soc. 81, 103850 https://doi.org/10.1016/j.scs.2022.103850.

Gani, S., Bhandari, S., Seraj, S., Wang, D.S., Patel, K., Soni, P., Arub, Z., Habib, G., Hildebrandt Ruiz, L., Apte, J.S., 2019. Submicron aerosol composition in the world's most polluted megacity: the Delhi aerosol supersite study. Atmos. Chem. Phys. 19, 6843–6859. https://doi.org/10.5194/acp-19-6843-2019.

Genc, D.D., Yesilyurt, C., Tuncel, G., 2010. Air pollution forecasting in Ankara, Turkey using air pollution index and its relation to assimilative capacity of the atmosphere. Environ. Monit. Assess. 166, 11–27. https://doi.org/10.1007/s10661-009-0981-y.

Hamada, S., Ohta, T., 2010. Seasonal variations in the cooling effect of urban green areas on surrounding urban areas. Urban For. Urban Green. 9, 15–24. https://doi.org/10.1016/j.ufug.2009.10.002.

Herath, P., Thatcher, M., Jin, H., Bai, X., 2021. Effectiveness of urban surface characteristics as mitigation strategies for the excessive summer heat in cities. Sustain. Cities Soc. 72, 103072 https://doi.org/10.1016/j.scs.2021.103072.

Holzworth, G.C., 1967. Mixing depths, wind speeds and air pollution potential for selected locations in the United States. J. Appl. Meteorol. 6, 1039–1044. https://doi.org/10.1175/1520-0450(1967)006<1039:MDWSAA>2.0.CO;2.

Hou, X., Fei, D., Kang, H., Zhang, Y., Gao, J., 2018. Seasonal statistical analysis of the impact of meteorological factors on fine particle pollution in China in 2013–2017. Nat. Hazards 93, 677–698. https://doi.org/10.1007/s11069-018-3315-y.

Imran, H.M., Kala, J., Ng, A.W.M., Muthukumaran, S., 2018. Effectiveness of green and cool roofs in mitigating urban heat island effects during a heatwave event in the city of Melbourne in Southeast Australia. J. Clean. Prod. 197, 393–405. https://doi.org/10.1016/j.jclepro.2018.06.179.

Imran, H.M., Kala, J., Ng, A.W.M., Muthukumaran, S., 2019. Effectiveness of vegetated patches as green infrastructure in mitigating urban Heat Island effects during a heatwave event in the city of Melbourne. Weather Clim. Extremes 25, 100217. https://doi.org/10.1016/j.wace.2019.100217.

IPCC, 2023. Sixth Assessment Report. https://www.ipcc.ch/assessment-report/ar6/ (accessed 7th August 2023).

Jacobs, S.J., Gallant, A.J.E., Tapper, N.J., Li, D., 2018. Use of cool roofs and vegetation to mitigate urban heat and improve human thermal stress in Melbourne, Australia. J. Appl. Meteorol. Climatol. 57, 1747–1764. https://doi.org/10.1175/JAMC-D-17-0243.1.

Janjic, Zavisa I., 1994. The Step–Mountain Eta Coordinate Model: Further developments of the convection, viscous sublayer, and turbulence closure schemes. Mon. Weather Rev. 122, 927–945. https://doi.org/10.1175/1520-0493(1994)122%3c0927:TSMECM%3e2.0.CO;2.

Khan, A., Papazoglou, E.G., Cartalis, C., Philippopoulos, K., Vasilakopoulou, K., Santamouris, M., 2022. On the mitigation potential and urban climate impact of increased green infrastructures in a coastal mediterranean city. Build. Environ. 221, 109264 https://doi.org/10.1016/j.buildenv.2022.109264.

Klein, P.M., Coffman, R., 2015. Establishment and performance of an experimental green roof under extreme climatic conditions. Sci. Total Environ. 512–513, 82–93. https://doi.org/10.1016/j.scitotenv.2015.01.020.

Klingberg, J., Broberg, M., Strandberg, B., Thorsson, P., Pleijel, H., 2017. Influence of urban vegetation on air pollution and noise exposure – a case study in Gothenburg, Sweden. Sci. Total Environ. 599–600, 1728–1739. https://doi.org/10.1016/j.scitotenv.2017.05.051.

Krayenhoff, E.S., Broadbent, A.M., Zhao, L., Georgescu, M., Middel, A., Voogt, J.A., Martilli, A., Sailor, D.J., Erell, E., 2021. Cooling hot cities: a systematic and critical review of the numerical modelling literature. Environ. Res. Lett. 16, 053007 https://doi.org/10.1088/1748-9326/abdcf1.

Kusaka, H., Kimura, F., 2004. Coupling a single-layer urban canopy model with a simple atmospheric model: impact on urban Heat Island simulation for an idealized case. J. Meteorol. Soc. Jpn. 82, 67–80. https://doi.org/10.2151/jmsj.82.67.

Kusaka, H., Kondo, H., Kikegawa, Y., Kimura, F., 2001. A simple single-layer urban canopy model for atmospheric models: comparison with multi-layer and slab models. Bound.-Layer Meteorol. 101, 329–358. https://doi.org/10.1023/A:1019207923078.

Lai, D., Liu, W., Gan, T., Liu, K., Chen, Q., 2019. A review of mitigating strategies to improve the thermal environment and thermal comfort in urban outdoor spaces. Sci. Total Environ. 661, 337–353. https://doi.org/10.1016/j.scitotenv.2019.01.062.

Li, X.-X., Norford, L.K., 2016. Evaluation of cool roof and vegetations in mitigating urban heat island in a tropical city, Singapore. Urban Clim. 16, 59–74. https://doi.org/10.1016/j.uclim.2015.12.002.

Liu, N., Morawska, L., 2020. Modeling the urban heat island mitigation effect of cool coatings in realistic urban morphology. J. Clean. Prod. 264, 121560 https://doi.org/10.1016/j.jclepro.2020.121560.

Liu, Y., Tang, G., Zhou, L., Hu, B., Liu, B., Li, Y., Liu, S., Wang, Y., 2019. Mixing layer transport flux of particulate matter in Beijing, China. Atmos. Chem. Phys. 19, 9531–9540. https://doi.org/10.5194/acp-19-9531-2019.

Livada, I., Pyrgou, A., Haddad, S., Sadeghi, M., Santamouris, M., 2021. Recent climatic trends and analysis of monthly heating and cooling degree hours in Sydney. Climate 9, 114. https://doi.org/10.3390/cli9070114.

Lu, C., Deng, Q., Liu, W., Huang, B., Shi, L., 2012. Characteristics of ventilation coefficient and its impact on urban air pollution. J. Cent. S. Univ. Technol. 19, 615–622. https://doi.org/10.1007/s11771-012-1047-9.

Lynn, B.H., Lynn, I.M., 2020. The impact of cool and green roofs on summertime temperatures in the cities of Jerusalem and Tel Aviv. Sci. Total Environ. 743, 140568 https://doi.org/10.1016/j.scitotenv.2020.140568.

Macintyre, H.L., Heaviside, C., 2019. Potential benefits of cool roofs in reducing heat-related mortality during heatwaves in a European city. Environ. Int. 127, 430–441. https://doi.org/10.1016/j.envint.2019.02.065.

Macintyre, H.L., Heaviside, C., Cai, X., Phalkey, R., 2021. Comparing temperature-related mortality impacts of cool roofs in winter and summer in a highly urbanized European region for present and future climate. Environ. Int. 154, 106606 https://doi.org/10.1016/j.envint.2021.106606.

Martilli, A., Clappier, A., Rotach, M.W., 2002. An urban surface exchange parameterisation for mesoscale models. Bound.-Layer Meteorol. 104, 261–304. https://doi.org/10.1023/A:1016099921195.

McRae, I., Freedman, F., Rivera, A., Li, X., Dou, J., Cruz, I., Ren, C., Dronova, I., Fraker, H., Bornstein, R., 2020. Integration of the WUDAPT, WRF, and ENVI-met models to simulate extreme daytime temperature mitigation strategies in San Jose. California. Build. Environ. 184, 107180 https://doi.org/10.1016/j.buildenv.2020.107180.

Mughal, M.O., Li, X., Yin, T., Martilli, A., Brousse, O., Dissegna, M.A., Norford, L.K., 2019. High-resolution, multilayer modeling of Singapore's urban climate incorporating local climate zones. JGR-Atmos. 124, 7764–7785. https://doi.org/10.1029/2018JD029796.

Mughal, M.O., Li, X.-X., Norford, L.K., 2020. Urban heat island mitigation in Singapore: evaluation using WRF/multilayer urban canopy model and local climate zones. Urban Clim. 34, 100714 https://doi.org/10.1016/j.uclim.2020.100714.

National Centers For Environmental Prediction/National Weather Service/NOAA/U.S. Department Of Commerce, 2015. NCEP gdas/fnl 0.25 degree global tropospheric analyses and forecast grids [dataset]. https://doi.org/10.5065/D65Q4T4Z.

Patel, P., Karmakar, S., Ghosh, S., Niyogi, D., 2020. Improved simulation of very heavy rainfall events by incorporating WUDAPT urban land use/land cover in WRF. Urban Clim. 32, 100616 https://doi.org/10.1016/j.uclim.2020.100616.

Potchter, O., Cohen, P., Bitan, A., 2006. Climatic behavior of various urban parks during hot and humid summer in the mediterranean city of Tel Aviv, Israel. Int. J. Climatol. 26, 1695–1711. https://doi.org/10.1002/joc.1330.

Rajeswari, J.R., Srinivas, C.V., Venkatraman, B., 2022. Impact of urbanization on boundary-layer parameters and mesoscale circulations over tropical coastal city. Chennai. Meteorol. Atmos. Phys. 134, 3. https://doi.org/10.1007/s00703-021-00843-9.

Ribeiro, I., Martilli, A., Falls, M., Zonato, A., Villalba, G., 2021. Highly resolved WRF-BEP/BEM simulations over Barcelona urban area with LCZ. Atmos. Res. 248, 105220 https://doi.org/10.1016/j.atmosres.2020.105220.

Saha, D., Soni, K., Mohanan, M.N., Singh, M., 2019. Long-term trend of ventilation coefficient over Delhi and its potential impacts on air quality. Remote Sens. Appl. Soc. Environ. 15, 100234 https://doi.org/10.1016/j.rsase.2019.05.003.

Salamanca, F., Martilli, A., 2010. A new building energy model coupled with an urban canopy parameterization for urban climate simulations—part II. Validation with one dimension off-line simulations. Theor. Appl. Climatol. 99, 345–356. https://doi.org/10.1007/s00704-009-0143-8.

Salata, F., Falasca, S., Ciancio, V., Curci, G., De Wilde, P., 2023. Climate-change related evolution of future building cooling energy demand in a Mediterranean country. Energ. Buildings 290, 113112. https://doi.org/10.1016/j.enbuild.2023.113112.

Santamouris, M., 2020. Recent progress on urban overheating and heat island research. Integrated assessment of the energy, environmental, vulnerability and health impact. Synergies with the global climate change. Energ. Buildings 207, 109482. https://doi.org/10.1016/j.enbuild.2019.109482.

Santamouris, M., Osmond, P., 2020. Increasing green infrastructure in cities: impact on ambient temperature, air quality and heat-related mortality and morbidity. Buildings 10, 233. https://doi.org/10.3390/buildings10120233.

Schinasi, L.H., Benmarhnia, T., De Roos, A.J., 2018. Modification of the association between high ambient temperature and health by urban microclimate indicators: a systematic review and meta-analysis. Environ. Res. 161, 168–180. https://doi.org/10.1016/j.envres.2017.11.004.

Segura, R., Badia, A., Ventura, S., Gilabert, J., Martilli, A., Villalba, G., 2021. Sensitivity study of PBL schemes and soil initialization using the WRF-BEP-BEM model over a Mediterranean coastal city. Urban Clim. 39, 100982 https://doi.org/10.1016/j.uclim.2021.100982.

Shi, Y., Han, Z., Xu, Y., Xiao, C., 2021. Impacts of climate change on heating and cooling degree-hours over China. Int. J. Climatol. 41, 1571–1583. https://doi.org/10.1002/joc.6889.

Shiflett, S.A., Liang, L.L., Crum, S.M., Feyisa, G.L., Wang, J., Jenerette, G.D., 2017. Variation in the urban vegetation, surface temperature, air temperature nexus. Sci. Total Environ. 579, 495–505. https://doi.org/10.1016/j.scitotenv.2016.11.069.

Shukla, K.K., Sarangi, C., Attada, R., Kumar, P., 2022. Characteristic dissimilarities during high aerosol loading days between western and eastern indo-Gangetic plain. Atmos. Environ. 269, 118837 https://doi.org/10.1016/j.atmosenv.2021.118837.

Skamarock, W.C., Klemp, J.B., Dudhia, J., Gill, D.O., Liu, Z., Berner, J., Wang, W., Powers, J.G., Duda, M.G., Barker, D.M., Huang, X.-Y., 2019. A description of the advanced research WRF model version 4. UCAR/NCAR. https://doi.org/10.5065/1DFH-6P97.

Srivastava, S., Lal, S., Subrahamanyam, D.B., Gupta, S., Venkataramani, S., Rajesh, T.A., 2010. Seasonal variability in mixed layer height and its impact on trace gas distribution over a tropical urban site: Ahmedabad. Atmos. Res. 96, 79–87. https://doi.org/10.1016/j.atmosres.2009.11.015.

Stewart, I.D., Oke, T.R., 2012. Local climate zones for urban temperature studies. Bull. Am. Meteorol. Soc. 93, 1879–1900. https://doi.org/10.1175/BAMS-D-11-00019.1.

Stull, R.B. (Ed.), 1988. An Introduction to Boundary Layer Meteorology. Springer, Netherlands, Dordrecht. https://doi.org/10.1007/978-94-009-3027-8.

Sun, X., Zhao, T., Xu, X., Bai, Y., Zhao, Y., Ma, X., Shu, Z., Hu, W., 2023. Identifying the impacts of warming anomalies in the Arctic region and the Tibetan plateau on PM2.5 pollution and regional transport over China. Atmos. Res. 294, 106966 https://doi.org/10.1016/j.atmosres.2023.106966.

Sussman, H.S., Dai, A., Raghavendra, A., Zhou, L., 2024. An evaluation of WRF urban canopy models over Bengaluru. India. Model. Earth Syst. Environ. 10, 1783–1802. https://doi.org/10.1007/s40808-023-01858-4.

UNI, 2014. UNI/TS 11300-1. Energy performance of buildings - Part 1.

Wang, C., Ren, Z., Dong, Y., Zhang, P., Guo, Y., Wang, W., Bao, G., 2022a. Efficient cooling of cities at global scale using urban green space to mitigate urban heat island effects in different climatic regions. Urban For. Urban Green. 74, 127635 https://doi.org/10.1016/j.ufug.2022.127635.

Wang, J., Hu, X.-M., 2020. Evaluating the performance of WRF urban schemes and PBL schemes over Dallas Fort Worth during a dry summer and a wet summer. J. Appl. Meteorol. Climatol. https://doi.org/10.1175/JAMC-D-19-0195.1.

Wang, X., Li, H., Sodoudi, S., 2022b. The effectiveness of cool and green roofs in mitigating urban heat island and improving human thermal comfort. Build. Environ. 217, 109082 https://doi.org/10.1016/j.buildenv.2022.109082.

Wilson, E., 1992. (1984) Biophilia, vol. 1. Harvard University Press, Cambridge (MA), p. 79.

Zhu, D., Ooka, R., 2023. WRF-based scenario experiment research on urban heat island: a review. Urban Clim. 49, 101512 https://doi.org/10.1016/j.uclim.2023.101512.